

# A NEW METHOD OF ACQUIRING FAST BEAM TRANSVERSAL PROFILE IN THE STORAGE RING\*

C. C. Cheng, Y. Y. Xiao, B.G. Sun<sup>#</sup>, Y. L. Yang, Z.R. Zhou, P. Lu, F. F. Wu, J. Y. Zou, K. Tang  
School of Nuclear Science and Technology & National Synchrotron Radiation Laboratory,  
University of Science and Technology of China, Hefei, 230029, China

## Abstract

A new method of acquiring fast beam transverse profile has been developed and will be used in HLS II. This method is based on four signals from MAPMT (multi-anode photo-multiplier tube) and logarithm processing technique. First, the calculation formula of beam transversal size and position are deduced using above method. Then, the main performances (e.g. sensitivity and linearity range) are analyzed. According to stimulation result, regardless of cross-talk and inconsistency between channels, the size signal has a linear relation with size  $\sigma$  when  $\sigma=0.8-2\text{mm}$  and position  $\delta=\pm 2\text{mm}$ , the position signal has a linear relation with position  $\delta$  and the linear range exceeds  $\pm 2\text{mm}$  when  $\sigma=0.8-2\text{mm}$ . With channel cross-talk and channel inconsistency being considered, the stimulation results also are given. Finally, a fast beam transverse profile monitor is designed and provides turn-by-turn measurement of the beam transverse profile.

## INTRODUCTION

In order to improve performance and commissioning instability of the Electron Storage Ring, it's necessary to study the beam dynamics, beam-beam interaction, etc. In these studies, beam transversal parameters change in a few turns. Although there have been several schemes, for example, beam position monitor (BPM) measurement system with turn-by-turn measurement ability [1] and beam transverse feedback system with bunch-by-bunch measurement ability [2] to measure the change of beam centres of mass. They can't be used to measure turn-by-turn or bunch-by-bunch transverse beam profile.

Traditional method of reconstructing transversal beam profile is Gaussian fitting [3-4], which needs dozens of channels of profile information to be sampled in parallel. As a result, costs and complexity are hugely increased.

This method needs only four electrode signals from an MAPMT to acquire beam profile and it has a highly precision measurement result after calibrating.

## DIAGRAM OF THE SYSTEM

The system mainly consists of two parts, one is optics system and the other is data acquisition and processing system.

To catch the profile of the synchrotron radiation light, MAPMT with the part number R5900U-00-L16 is used as the front-end optical detector. It is a 16-channel linear array photoelectric converter characterized by excellent

response performance with rise time  $\sim 0.6\text{ns}$ . Synchrotron light is divided to horizontal and vertical directions with an optics system and then is received, respectively. Four channel photocurrent signals are conditioned by signal conditioning circuit before they are sent into a high-speed ADC module. In the end, Xilinx Virtex-5 series FPGA chip is used to sample discrete data from ADC and perform high speed logarithm processing operation.

The schematic block diagram of the system is shown in Fig. 1.

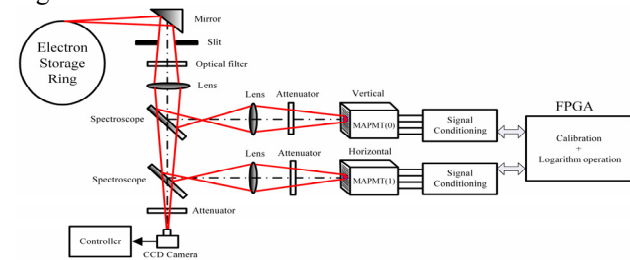


Figure 1: Block diagram of the system.

## THEORY

According to the knowledge of the physics of electron storage rings, electron radiates synchrotron light when passing through the bend-magnetic and the light presents a Gaussian distribution in transverse plane. So we assume synchrotron light intensity distribution function:

$$\Phi(x) = \Phi_0 e^{-\frac{(x-\delta)^2}{2\sigma^2}} \quad (1)$$

Where,  $\Phi_0$  is the peak light intensity;  $\delta$  is beam position that synchrotron light centre offsets the specified centre of the MAPMT;  $\sigma$  is beam size which roughly varies from 0.8mm to 2mm.

With the parameters of MAPMT, the synchrotron light distribution is shown in Fig. 2.

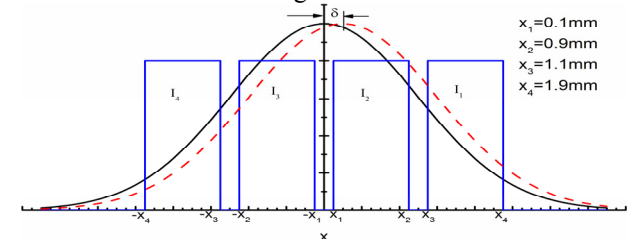


Figure 2: Light intensity distribution at MAPMT.

Figure 2 shows that photocurrent from four channels is proportional to the integral of light intensity and they can be expressed by the subtraction of two error functions shown in Eq.2.

\*Work supported by the National Science Foundation of China (11175173, 11105141)

<sup>#</sup> E-mail: bgsun@ustc.edu.cn

$$\begin{cases} I_1 = \int_{x_3}^{x_4} \Phi(x)dx = I_0 \left[ \operatorname{erf}\left(\frac{x_4 - \delta}{\sqrt{2}\sigma}\right) - \operatorname{erf}\left(\frac{x_3 - \delta}{\sqrt{2}\sigma}\right) \right] \\ I_2 = \int_{x_1}^{x_2} \Phi(x)dx = I_0 \left[ \operatorname{erf}\left(\frac{x_2 - \delta}{\sqrt{2}\sigma}\right) - \operatorname{erf}\left(\frac{x_1 - \delta}{\sqrt{2}\sigma}\right) \right] \\ I_3 = \int_{-x_2}^{-x_1} \Phi(x)dx = I_0 \left[ \operatorname{erf}\left(\frac{-x_1 - \delta}{\sqrt{2}\sigma}\right) - \operatorname{erf}\left(\frac{-x_2 - \delta}{\sqrt{2}\sigma}\right) \right] \\ I_4 = \int_{-x_4}^{-x_3} \Phi(x)dx = I_0 \left[ \operatorname{erf}\left(\frac{-x_3 - \delta}{\sqrt{2}\sigma}\right) - \operatorname{erf}\left(\frac{-x_4 - \delta}{\sqrt{2}\sigma}\right) \right] \end{cases} \quad (2)$$

In ideal condition when the four continuous channel electrodes have the same response characteristic, beam size signal and position signal are shown in Eq.3.

$$\begin{cases} S_{\ln}(\sigma, \delta) = \left( \frac{1}{\ln(I_2) + \ln(I_3) - \ln(I_1) - \ln(I_4)} \right)^{1/2} = \left( \ln \frac{I_2 I_3}{I_1 I_4} \right)^{-1/2} \\ P_{\ln}(\sigma, \delta) = \frac{\ln(I_1) + \ln(I_2) - \ln(I_3) - \ln(I_4)}{\ln(I_2) + \ln(I_3) - \ln(I_1) - \ln(I_4)} = \frac{\ln \frac{I_1 I_2}{I_3 I_4}}{\ln \frac{I_2 I_3}{I_1 I_4}} \end{cases} \quad (3)$$

After putting the integral result in Eq.2 into Eq.3 and simplifying it, we can obtain how the size signal and the position signal vary from size and position. The results are shown in Fig. 3 and Fig. 4.

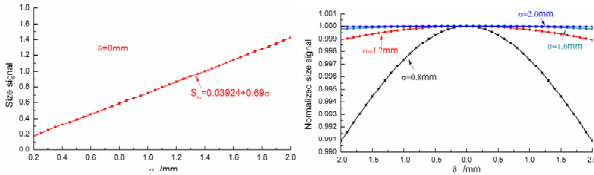


Figure 3: Size signal vs. size and position.

When  $\delta=0\text{mm}$  and  $\sigma=0.2\sim 2\text{mm}$ , size signal has a good linear relation with size and the linear fitting equation is  $S_{\ln}(\sigma)=0.03924+0.69\sigma$ . When  $\sigma=0.8\sim 2\text{mm}$ , position  $\delta$  has an effect on normalized ideal size signal within 1%.

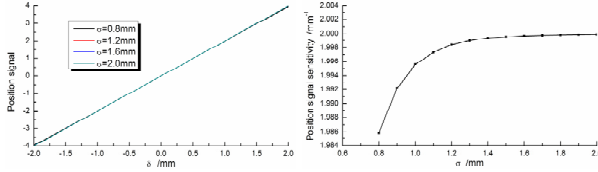


Figure 4: Position signal vs. position and size.

When  $\sigma=0.8\sim 2\text{mm}$ , position signal has a good linear relation with position with  $\delta=\pm 2\text{mm}$  and size has an impact on position signal sensitivity within 1%.

### Calibration

In practical use, cross-talk and inconsistency between channels always exist. So we establish a linear model based on the response characteristics of MAPMT to simplify and analyze actual photocurrent signals. We suppose  $\hat{I}_1, \hat{I}_2, \hat{I}_3$  and  $\hat{I}_4$  to represent actual photocurrent signals which are integral of light intensity multiplied by normalized gain factor  $g_i(i=1,2,3,4)$ . According to Eq.3, actual size signal  $\hat{S}_{\ln}(\sigma, \delta)$  and position signal  $\hat{P}_{\ln}(\sigma, \delta)$  are described as Eq.4.

$$\begin{cases} \hat{S}_{\ln}(\sigma, \delta) = \left( \ln \frac{\hat{I}_2 \hat{I}_3}{\hat{I}_1 \hat{I}_4} \right)^{-1/2} = \left( \ln \frac{g_2 g_3}{g_1 g_4} + \ln \frac{I_2 I_3}{I_1 I_4} \right)^{-1/2} \\ \hat{P}_{\ln}(\sigma, \delta) = \frac{\ln \frac{\hat{I}_1 \hat{I}_2}{\hat{I}_3 \hat{I}_4}}{\ln \frac{\hat{I}_2 \hat{I}_3}{\hat{I}_1 \hat{I}_4}} = \frac{\ln \frac{g_1 g_2}{g_3 g_4} + \ln \frac{I_1 I_2}{I_3 I_4}}{\ln \frac{g_2 g_3}{g_1 g_4} + \ln \frac{I_2 I_3}{I_1 I_4}} \end{cases} \quad (4)$$

In fact, Eq.3 can be viewed as a special case of Eq.4 when  $g_1=g_2=g_3=g_4=1$ . In Eq.4, We assume theoretical gain correction factor  $d_s = \ln \frac{g_2 g_3}{g_1 g_4}$ ,  $d_p = \ln \frac{g_1 g_2}{g_3 g_4}$ . Then we can get:

$$\begin{cases} \hat{S}_{\ln}(\sigma, \delta) = S_{\ln}(\sigma, \delta) [1 + d_s S_{\ln}^2(\sigma, \delta)]^{-1/2} \\ \hat{P}_{\ln}(\sigma, \delta) = P_{\ln}(\sigma, \delta) [1 + d_s S_{\ln}^2(\sigma, \delta)]^{-1} + d_p S_{\ln}^2(\sigma, \delta) [1 + d_s S_{\ln}^2(\sigma, \delta)]^{-1} \end{cases} \quad (5)$$

According to the simulation result above that position has little influence on ideal size signal and it is true for size to ideal position signal, so we can get

$$\begin{cases} S_{\ln}(\sigma, \delta) \approx S_{\ln}(\sigma) \\ P_{\ln}(\sigma, \delta) \approx P_{\ln}(\delta) \end{cases} \quad (6)$$

Therefore, Eq.5 becomes the form described in Eq.7.

$$\begin{cases} \hat{S}_{\ln}(\sigma, \delta) \approx S_{\ln}(\sigma) [1 + \tilde{d}_s S_{\ln}^2(\sigma)]^{-1/2} \\ \hat{P}_{\ln}(\sigma, \delta) \approx P_{\ln}(\delta) [1 + \tilde{d}_s S_{\ln}^2(\sigma)]^{-1} + \tilde{d}_p S_{\ln}^2(\sigma) [1 + \tilde{d}_s S_{\ln}^2(\sigma)]^{-1} \end{cases} \quad (7)$$

Where,  $\tilde{d}_s$  and  $\tilde{d}_p$  are actual gain correction factors.

From the Eq.7, we know that actual size signal has a remarkable nonlinear relation with size  $\sigma$ ; actual position signal has a good relation with position  $\delta$ . After the actual gain correction factors are measured, modified size signal  $\tilde{S}_{\ln}(\sigma, \delta)$  and modified position signal  $\tilde{P}_{\ln}(\sigma, \delta)$  can be expressed in Eq.8.

$$\begin{cases} \tilde{S}_{\ln}(\sigma, \delta) = \left( \ln \frac{\hat{I}_2 \hat{I}_3}{\hat{I}_1 \hat{I}_4} - \tilde{d}_s \right)^{-1/2} \\ \tilde{P}_{\ln}(\sigma, \delta) = \frac{\ln \frac{\hat{I}_1 \hat{I}_2}{\hat{I}_3 \hat{I}_4} - \tilde{d}_p}{\ln \frac{\hat{I}_2 \hat{I}_3}{\hat{I}_1 \hat{I}_4} - \tilde{d}_s} \end{cases} \quad (8)$$

The process of deducing modified size signal and modified position signal is based on the assumption shown in Eq.6. In order to prove that the assumption is reasonable and effective, we consider the worst case that the four normalized gain factor  $g_i(i=1,2,3,4)$  deviation is within 5%, i.e.  $g_1=1.05, g_2=1, g_3=0.95, g_4=1.05$  and then discuss how much the modified size signal diverges from ideal size signal and modified position signal diverges from ideal position signal.

APPLICATION

According to the depict above, in the worst case when  $g_1=1.05, g_2=1, g_3=0.95, g_4=1.05$ , the theoretical channel gain correction factors of  $d_s$  is  $-0.1489$  and  $d_p$  is  $0.05129$ .

When  $\sigma=0.8-2\text{mm}$ , we can obtain ideal size signal from ideal size signal fitting equation. Then with the slope and intercept of actual position signal shown in Eq.7 being calculated, we can get the actual gain correction factors and how the position signal sensitivity varies from the size. The results are shown in Fig. 5 and Fig. 6.

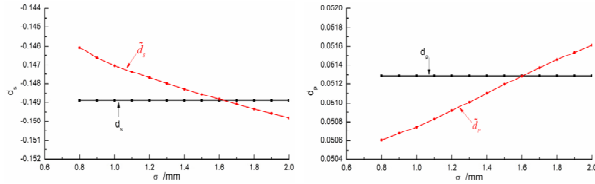


Figure 5: Channel gain correction factors vs. size.

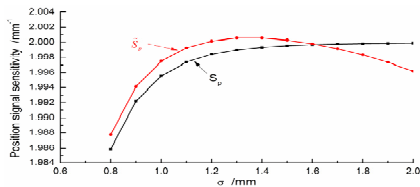


Figure 6: Position signal sensitivity vs. size.

Figure 5 tells us that actual channel gain correction factors plotted in red line is almost closed to theoretical value and the relative error is within  $\pm 0.1\%$  when size  $\sigma=1.6\text{mm}$ . And the size will be chosen as the synchrotron light size to calibrate the channel difference.

From Fig. 6, actual position signal sensitivity denoted in red approximates to theoretical simulation result, and they all roughly equals to 2 when size  $\sigma=0.8-2\text{mm}$ . The maximum error is within  $0.7\%$ .

Before channel gain being modified, according to Eq.4, we can get how the size signal and position signal change with size and position. The results are shown in Fig. 7.

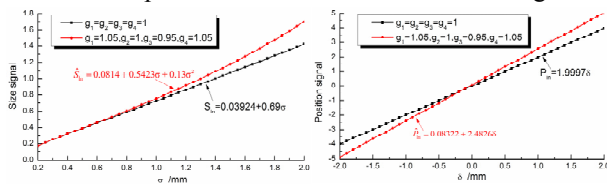


Figure 7: Size signal vs. size and position vs. position.

From Fig. 7, we know linear range of size signal is about  $0.2-0.8\text{mm}$  before calibrating. But it presents a huge nonlinear relation with size  $\sigma$  when size gradually increases from  $0.8\text{mm}$  to  $2\text{mm}$ . The maximum relative error is almost up to  $20\%$  when  $\sigma=2\text{mm}$ . In contrast, the quadratic curve fitting equation is also given.

On the contrary, position signal presents a good linear relation with position even there exists channel difference. However, the slope of it deviates from the ideal slope with relative error up to  $24\%$ , which will cause large error without calibrating.

After actual channel gain correction factor being worked out with beam transverse profile measurement system [5], then we put them into Eq.8. As a result, we can obtain how the modified size signal and modified

position signal vary from beam size and position. The results are plotted in Fig. 8.

Figure 8 shows that the modified size signal has a good linear relation with size and linear range exceeds  $1.8\text{mm}$ , meanwhile the relative error is less than  $0.01\%$  compared with ideal linear fitting result when size  $\sigma=0.2-2\text{mm}$ . The slope of modified size signal is much closed to ideal slope and the relative error is also less than  $0.01\%$ .

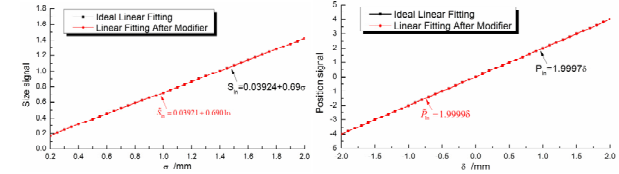


Figure 8: Modified size signal vs. size and modified position signal vs. position.

According to the simulation result described above, we can gather them to obtain the position signal sensitivity and size signal linear range on the whole shown in table 1. Table 1: Summary of position signal sensitivity and size signal linear range in three modes.

Mode	Sensitivity (mm <sup>-1</sup> )	Linear range(mm)
Ideal condition	1.9997	1.8
Before calibration	2.4826	0.6
After calibration	1.9999	1.8

From the result, we know that before calibration, position signal sensitivity hugely deviates from the ideal fitting result and size signal linear range is only  $0.6\text{mm}$ ; after calibration, position signal sensitivity is almost equal to ideal fitting result, and size signal linear range also reaches  $1.8\text{mm}$  compared with ideal fitting result. So calibration greatly improves the measurement accuracy.

CONCLUSION

The method needs only four channel electrode signals and adopts logarithm processing technique to measure turn-by-turn beam transverse profile. It owns a precision measurement result that relative error is less than  $0.01\%$  compared with ideal fitting result after calibrating.

REFERENCES

- [1] M.G. Billing, et al. "Investigations of Injection Orbits at CESR Based on Turn-By-Turn BPM Measurements". PAC'05, Knoxville, 2005, p.1228.
- [2] Z.R. Zhou, et al. "Commissioning of the Digital Transverse Bunch-by-Bunch Feedback System for the HLS". PAC'09, TH6REP084, 2009, p.278.
- [3] M. Palmer, et al. "Design and Implementation of an Electron and Positron Multibunch Turn-by-turn Vertical Beam Profile Monitor in CESR". PAC'07, FRPMS047, 2007, p.4081.
- [4] A.V. Bogomyagkov, et al. "New Fast Beam Profile Monitor for Electron-positron Colliders". Review of Scientific Instruments, Vol. 78, 2007, 043305:1-6.
- [5] K.R. Ye, et al. "Synchrotron Radiation Monitor and Mirror at SSRF". DIPAC'09, TUPD37, 2009, p.381.